ACS Catalysis

Research Article

pubs.acs.org/acscatalysis

Surface Composition and Lattice Ordering-Controlled Activity and Durability of CuPt Electrocatalysts for Oxygen Reduction Reaction

Chun-Hua Cui,[†] Hui-Hui Li,[‡] Xiao-Jing Liu,[‡] Min-Rui Gao,[†] and Shu-Hong Yu*[,†,‡]

[†]Division of Nanomaterials and Chemistry, Hefei National Laboratory for Physical Sciences at Microscale, and [‡]Department of Chemistry and the National Synchrotron Radiation Laboratory, University of Science and Technology of China, Hefei 230026, P. R. China

Supporting Information

ABSTRACT: We report the enhanced activity and stability of CuPt bimetallic tubular electrocatalysts through potential cycling in acidic electrolyte. A series of CuPt tubular electrocatalysts with sequential increased lattice ordering and surface atomic fraction of Pt were designed and synthesized by thermal annealing to reveal their improved electrocatalytic properties. These low-Pt-content electrocatalysts with Pt shell are formed through the thermal annealing and following potential cycling treatment. The catalysts (C1) with a low atomic fraction of Pt on the surface and low lattice ordering in the bulk are treated in acidic electrolyte, resulting in the formation of a Pt shell with relatively low activity and stability. However, the catalysts (C2) with a Pt-rich surface and high lattice ordering have a highly enhanced electrochemical surface area after potential cycling via surface roughing. The rough Pt shell of the C2 catalysts is achieved by leaching of surface Cu and the concomitant morphology restructuring. The C2 Pt surface demonstrated highly improved specific and mass activities of 0.8 mA cm_{Pt}^{-2} and 0.232 A mg_{Pt}^{-1} at 0.9 V for oxygen reduction reaction (ORR), and after 10 000 cycles, the C2 catalysts display almost no loss of the initial electrochemical active surface area (ECSA). Meanwhile, the stability of these CuPt catalysts shows regular change. Moreover, after a long-term stability measurement, the ECSA of C2 catalysts can be restored to the initial value after another potential cycling treatment, and thus, this kind of electrocatalyst may be developed as next-generation restorable cathode fuel cell catalysts.

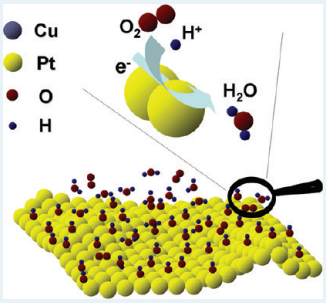

KEYWORDS: *CuPt, oxygen reduction, lattice ordering, morphology restructuring, potential cycling*

1. INTRODUCTION

The low catalytic activity and poor durability of platinum-containing catalysts for oxygen reduction reaction (ORR) and the high cost involved are major barriers for automotive and portable applications.[1−3] A number of strategies have been proposed to improve the catalytic activity and utilization on a tiny particle and one-dimensional nanostructure that involve dealloying of Pt to the formation of a Pt-shell surface,[4,5] depositing a monolayer of Pt on fine particles,[6,7] forming a Pt-rich surface by CO-adsorbate-induced segregation in alkaline electrolyte solution[8] and obtaining highly active, defect-free, ultrathin Pt, Pd, and PtPd nanowires by acid-treating and a surfactantless method,[9−13] In a strong acidic and hostile electrochemical environment, however, the stability of catalysts has been a serious issue preventing the wide use of this technology.

The Pt-based nanoparticle catalysts with decreased particle size to improve the utilization must suffer Ostwald ripening and particle coalescence caused surface area loss or particle growth for the primary degradation.[14,15] The nature of the particle catalyst degradation is that the surface free energy of most materials tends to the minimum, adapting their geometrical and electronic structure to the environments.[16] On the other hand, leaching of nonnoble metal atoms from bimetallic alloy catalysts should be another kind of serious degradation in an acidic electrolyte.[17,18] Therefore, incorporation of structure/morphology stability and the composition stability (decrease leaching of the nonnoble metals) into electrode materials, this kind of catalyst with high activity and stability is very promising.

Because restructuring on metal surfaces is a very common but particularly important phenomenon, it may be induced by adsorbates for a decrease in the surface free energy.[19−22] Generally, the rough or low coordination number surface with high surface energy will result in a decrease in the active surface area in an electrolyte due to morphology restructuring; for example, metal particle ripening.[16] In contrast, adsorbate-induced restructuring or surface segregation may rebuild or hinder the formation of a rough surface.[23−26] In electrolyte conditions, adsorbates such as OH^-, OOH^-, and O_2^- may induce surface segregation and restructuring.[15,23,27] Thus, the surface composition and morphology change under redox potential cycling should be of importance for understanding the improvement of activity and stability.

To study the configuration change of the catalytic surface in the electrolyte, the metal surface should be clean, and no surfactants should be used in synthesis.[28,29] A template-directed method and galvanic displacement synthesis of one-dimensional metallic catalysts have received increasing interest.[30−32] A

Received: January 26, 2012
Revised: March 8, 2012
Published: March 30, 2012

newly developed one-step nonaqueous solution electrochemical method was used to synthesize the tubular catalysts on an anodic aluminum oxide (AAO) template in anhydrous dimethyl sulfoxide (DMSO) medium without addition of any other surfactants.[33,34] The DMSO molecules can be washed away easily and cannot even be detected by X-ray photoelectron spectroscopy (XPS), so the synthesized materials are available for investigation of the surface chemistry.[35]

Herein, we demonstrate the effective design and synthesis of highly active and stable bimetallic CuPt electrocatalysts through potential cycling. To distinguish the different catalysts, the catalysts with Cu-rich and Pt-rich surfaces are abbreviated as C1 and C2, respectively. The as-treated C2 catalysts have a highly improved electrochemical active surface area (ECSA), and the Pt surfaces show a higher structure stability than those of the C1 catalysts, whereas the C2 catalysts with a Pt-rich surface and high lattice ordering could withstand the strong acid conditions and decrease the Cu leaching from the particles. The obtained rough Pt surfaces show a high activity and long-term durability for ORR. The specific activity for C2 catalysts is 0.8 mA cm^{-2} at 0.9 V, and it showed 5-fold more active ORR than that of the C1 catalysts. The C2 catalysts demonstrated a mass activity of 0.232 A mg^{-1} Pt at 0.9 V, which was a 7-fold higher activity than that of the C1 catalysts. Moreover, after stability measurement, these kinds of C2 catalysts can be restored after 250 cycles. This study will explain the origin of the improved catalytic stability.

2. EXPERIMENTAL SECTION

2.1. Chemicals. $NaNO_3$, CuBr, dimethyl sulfoxide (99% wt %), C_2H_5OH (99.7% wt %), $HClO_4$ (70−72 wt %), and NaOH were commercially available from Shanghai Chemical Reagent Co. Ltd.; Nafion (wt 5%), from Sigma-Aldrich; and $PtCl_2$, from J&K Chemical Ltd. All the chemical reagents were analytical grade and used as received without further purification.

2.2. Electrochemical Synthesis of Unsupported Porous CuPt Tubes. The commercial AAO template (Anodisc 47, Whatman Co., U.K.) with a channel diameter of ∼300 nm measured by scanning electron microscopy (SEM) was sputtered with a thin Au layer on one side, ∼40 nm thickness, to form an annular base electrode. This thin Au layer was used as a working electrode in the subsequent electrodeposition of the desired materials. For CuPt synthesis, the experiments were performed potentiostatically at −1.2 V versus Ag/AgCl (3 M) in anhydrous DMSO solvents mixed with 20 mM $PtCl_2$, 30 mM CuBr, and 100 mM $NaNO_3$. After synthesis, the thin Au layer on one side of the AAO template was erased completely by alumina particle, washed with doubly deionized H_2O and ethanol several times, and dried for annealing treatment. The AAO-template-supported CuPt material was loaded onto the bottom of a rectangular ceramic boat and then annealed to a maximum temperature of 300−700 °C (5 °C/min heating rate) in a flow tubular furnace (MTI GSL1400X) under a flowing 5% hydrogen atmosphere (Ar balance), then the products were exposed by immerging in 1.0 M NaOH solution for 1 h to completely remove the AAO template, followed by washing with doubly deionized H_2O and ethanol several times.

2.3. Materials Characterization. The resulting phase of the as-synthesized CuPt porous tubes was examined by X-ray diffraction (Cu K radiation, λ = 0.154 056 nm, 4°/min, range from 30 to 65°). X-ray photoemission spectrometer was recorded on an ESCALAB-MK-II using a Mg Kα radiation exciting source. Energy-dispersive X-ray spectra (EDX) were taken with a JEOJ-2010 transmission electron microscope with an acceleration voltage of 200 kV. SEM images were obtained with a Zeis Supra 40 high-resolution field emission scanning electron microscope operating at 5 kV. Transmission electron microscopy (TEM) and high-resolution TEM (HRTEM) images were obtained using a JEOL-2100F TEM with an acceleration voltage of 200 kV. Inductively coupled plasma mass spectrometry (ICP-MS) data were obtained by an Optima 7300 DV.

2.4. Electrochemical Measurements. *2.4.1. Electrochemical System and Rotating Disk Electrode Film Preparation.* The electrochemical measurements were investigated using a three-electrode system on an IM6ex electrochemical workstation (Zahner, Germany). A platinum foil and Ag/AgCl (3 M) were used as the counter and reference electrodes, respectively. All electrode potentials were recorded with respect to the reversible hydrogen electrode (RHE). A glassy carbon rotating disk electrode (RDE) (PINE, 5 mm diameter, 0.196 cm^2) was polished to a mirror finish and thoroughly cleaned. The preparation method of the working electrode is as follows: In short, ethanol suspensions of 1 mg catalyst (recorded with metal Pt) per milliliter with Nafion (diluted from 5 wt % Nafion, Sigma-Aldrich) were obtained by ultrasonic mixing for about 20 min. The metal catalyst suspension was transferred onto the RDE substrate, leading to a metal Pt loading of 32 $\mu g/cm^2$ for a series of unsupported CuPt catalysts. Finally, the as-prepared catalyst RDE was dried at room temperature.

2.4.2. Electrochemical Treatments. The electrochemical treatment process was conducted in Ar-saturated 0.1 M $HClO_4$ solution at a sweep rate of 250 mV/s at room temperature. The initial three cyclic voltammograms were recorded to monitor the surface Cu trace, then the catalysts were electrochemically treated between 0.05 and 1.2 V at a sweep rate of 250 mV/s for 250 cycles. For ECSA measurement, the sweep rate was changed at 50 mV/s from 0.05 to 1.2 V, and the electric quantity of H_{upd} adsorption/desorption region was calculated by the attached electrochemical analysis software package of the IM6ex electrochemical workstation.

2.4.3. OH_{ad}-Induced Electrochemical Treatments. To confirm the OH_{ad}-induced restructuring, the prepared RDE electrode performed at 250 mV/s from 0.05 to 1.2 V to record the first scan, and then the specified potential scans between 0.5 and 0.85 V at a sweep rate of 100 mV/s with different circles were performed. After the specified sweep circles, the potential was again scanned at 250 mV/s from 0.05 to 1.2 V, and the CV curves were recorded for comparison.

2.4.4. ORR Polarization. Polarization curves were obtained by a potential sweep from 0.3 to 1.05 V at a scan rate of 20 mV/s and rotation disk speed of 1600 rpm at room temperature. The specific and mass activities were studied at 0.9 V vs RHE.

2.4.5. Kinetic Current (j_k) calculation. The cyclic voltammetry measurements were performed in Ar-saturated or purged 0.1 M $HClO_4$ solutions at a sweep rate of 50 mV/s. The ECSA was calculated by measuring the areas of H desorption between 0.05 and 0.4 V versus RHE after the deduction of the double-layer region. By using the charge passed for H-desorption, Q_H, the ECSA of Pt can be calculated using the following equation:

$$\mathrm{ECSA} = \frac{Q_H}{m \times 0.21} \quad (1)$$

dx.doi.org/10.1021/cs300058c | ACS Catal. 2012, 2, 916−924

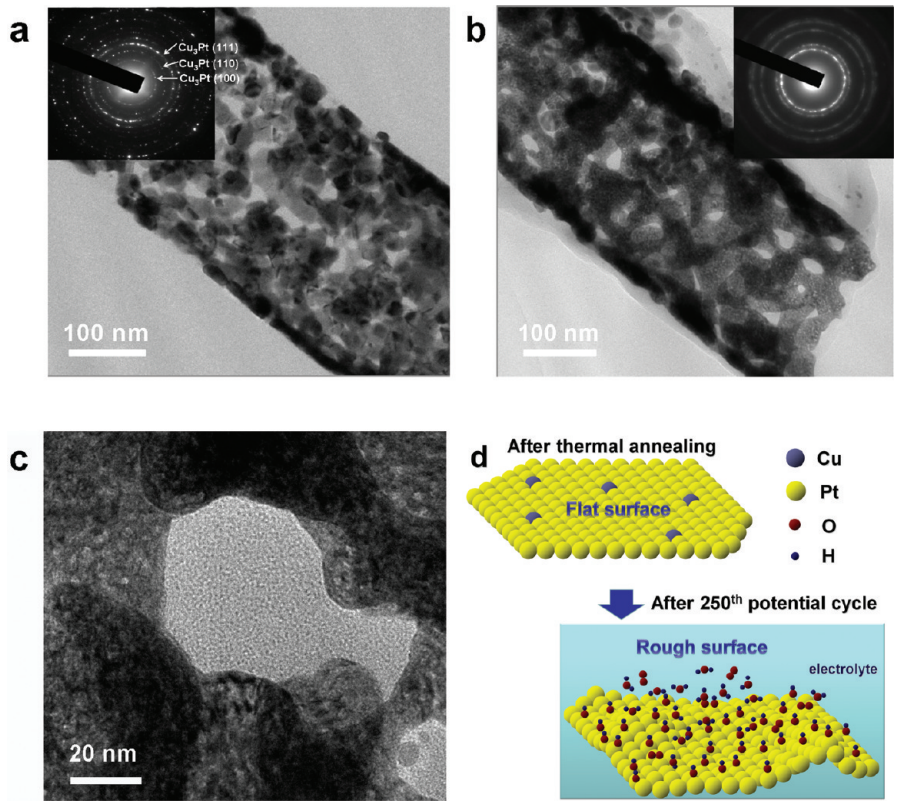

Figure 1. (a) TEM image of a part of a CuPt tube after annealing at 600 °C. (b) TEM image of a part of a CuPt restructured tube obtained after 250 cycles between 0.05 and 1.2 V vs RHE in Ar-saturated 0.1 M $HClO_4$ solutions. Insets are the ED patterns showing the order−disorder transformation before and after morphology restructuring. (c) Amplified TEM image shows the highly rough surface. (d) Schematic of surface evolution after 250 cycles.

where m represents the Pt loading (mg) in the electrode; Q_H, the charge for H-desorption (mC/cm^2); and 0.21, the charge required to oxidize a monolayer of H_2 on clean Pt.

Instead, for ORR measurements, the electrolyte was replaced with saturated oxygen, and the experiments were carried out using a RDE with a rotation rate of 1600 rpm and a sweep rate of 20 mV/s. The current densities were normalized to the geometric area of RDE, 0.196 cm^2.

The kinetic current,i_k, is expressed by the following equation:

$$\frac{1}{i} = \frac{1}{i_k} + \frac{1}{i_d} \tag{2}$$

where i is the measured current and i_d is the diffusion-limited current. Then, the specific current density, j_k, can be calculated from eq 2 when the measured real surface area, A_{real}, was obtained:

$$j_k = \frac{i_k}{A_{real}} = \frac{i_d \times i}{i_d - i} \times \frac{1}{A_{real}} \tag{3}$$

For each catalyst, specific and mass activities were obtained when the kinetic current was normalized to the ECSA and loading amount of metal, respectively.

3. RESULTS AND DISCUSSION

3.1. Synthesis and Structure of Cu−Pt Catalysts. To study the effects of crystal structure and surface composition on the electrocatalytic properties, we studied a series of CuPt bimetallic catalysts with a sequential increase in the surface atomic fraction of Pt on a mixed Cu−Pt surface and lattice ordering through different thermal annealing treatments. The CuPt nanoparticle tubular catalysts with ∼20 atom % Pt were synthesized by a newly developed electrochemical method.[33,34] After the synthesis, AAO template-supported annealing treatments with temperatures of 300, 500, 600, and 700 °C (denoted as CP3, CP5, CP6, and CP7, respectively) were performed under a flowing 5% hydrogen atmosphere to form a tubular structure.

The TEM image shows the nanoparticle tubular structure in Figure 1a. When annealing below 500 °C, the particle size is difficult to observe because of the unclear crystal boundary (Supporting Information, Figure S1). Upon annealing treatment, the Pt atoms strongly migrate to the outer surface because of the heat of segregation and the surface mixing energy,[5,35] so we can use the annealing temperature to control the atomic fraction of Pt on the surface.

This hypothesis has been easily proved by the cyclic voltammetry (CV) data in Figure 2a. The higher the temperature increases, the lower the Cu redox peaks on the particle surface decrease. The change trend of the initial three cycles can be examined (Supporting Information, Figure S2). There are quite weak Cu redox peaks when the temperature increases to 700 °C, suggesting the formation of Pt-rich surfaces. On the other hand, the atomic fraction of Pt in the surface region measured by XPS increases with an increase in the temperature in Figure 2b. These results indicate the increase of Pt atoms on the surface. In other words, more Cu atoms migrate into the core regions upon the annealing. The decrease in the Cu composition in the surface region reduces the relative peak intensity of the shakeup satellite of Cu2p, indicating the modification of the chemical environments and

dx.doi.org/10.1021/cs300058c | ACS Catal. 2012, 2, 916−924

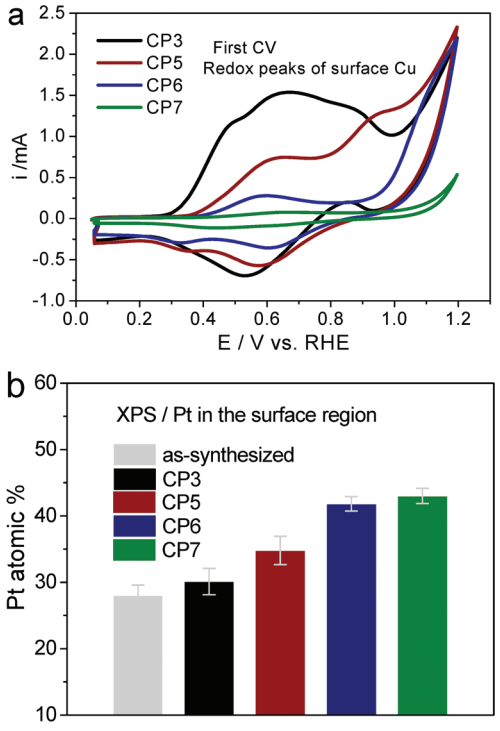

Figure 2. Relative composition change between Pt and Cu on topmost layer and in the surface region. (a) CVs of the catalysts were recorded with initial first cycle. The continuous decrease of the relative redox peak current intensities of Cu suggests the decrease in the surface Cu atomic fraction with an increase in the annealing temperature. (b) The Pt atomic fraction in the surface region increases with an increase in the annealing temperature measured by XPS.

electronic structure of Cu atoms (Supporting Information, Figure S3).

The HRTEM images show the appearance of the Cu_3Pt (100) and Cu_3Pt (111) planes and superlattices after thermal annealing (Supporting Information Figure S4). The results agree with the CuPt binary alloy phase diagrams.[36] The XRD data show that the Cu_3Pt(111) peaks become narrower, suggesting a larger particle size after annealing with higher temperature (Supporting Information Figure S5). Moreover, the XRD results show that the crystals experience a disorder−order transformation with an increase in the annealing temperature.

3.2. Composition after Potential Cycling Treatment. After annealing, the samples were cyclic voltammetrically treated in an Ar-saturated 0.1 M $HClO_4$ solution for 250 cycles at room temperature (Figure 3). Potential cycling can deplete the surface Cu of the catalysts. EDX and inductively coupled plasma mass spectrometry results indicate that the CP3 composition changed from $Cu_{80}Pt_{20}$ to $Cu_{52}Pt_{48}$ after cycling (Figure 4). This result is similar to the reported composition change from $Cu_{75}Pt_{25}$ to $Cu_{45}Pt_{55}$ after dealloying in the same potential region by Strasser et al.[37] When the temperature is increased to 500 °C for CP5, the composition changes from $Cu_{80}Pt_{20}$ to $Cu_{65}Pt_{35}$, suggesting less Cu was etched into solution. Notably, when the temperature is further increased to 700 °C for CP7, we can detect only quite weak Cu redox peaks by the magnified pattern (Supporting Information Figure S2d), so the atomic fraction of Pt on the surface is highly improved. It shows that the composition changes only from $Cu_{80}Pt_{20}$ to $Cu_{71}Pt_{29}$. XPS analyses showed that the composition ratio between Pt and Cu in the surface region for CP3 suffered a maximum change, but for CP7, it is nearly unchanged, in contrast to that before cycling (Figure 4). These results suggest that the high atomic fraction of Pt on the surface could prevent the leaching of Cu.

Stamenkovic and co-workers found that the pure Pt outermost layer could protect the subsurface transition metal atoms from dissolution.[18] Moreover, despite the formation of the Pt surface, when we continue the cycling, the atomic fraction of Cu for CP3 and CP5 will further decrease. The possible explanation may be that the Cu atoms in the subsurface or core region continuously migrate to the outer surface and dissolve into solution, which is also called surface segregation by Mayrhofer.[15] However, the composition ratios of CP6 and CP7 did not have an obvious change. This result was confirmed by ICP data. This issue may be attributed to the less surface segregation of Cu owing to the difference in bond energy or bond length between disordered and ordered alloys in terms of nearest-neighbor pair-bonding.[38,39] Therefore, the Pt-rich surface and high lattice ordering can prevent the leaching of Cu.

3.3. ECSA after Potential Cycling Treatment. Thermal annealing will cause the ripening and growth of the CuPt nanoparticles, and a higher temperature results in a larger particle size and, thus, decrease in the surface area per mass. However, in this experiment, after 250 potential cycles, the ECSAs of the samples increase with an increase in the temperature. The ECSAs for CP3, CP5, CP6, and CP7 are 19, 28.7, 32.3, and 31.8 $m^2\ g_{Pt}^{-1}$, respectively. The values of this unsupported CuPt nanoparticle tubular catalysts are even higher than that of fuel cell grade Pt black (about 19 $m^2\ g_{Pt}^{-1}$).[40] Here, we try to explain the reasons why a Pt-rich surface and ordered structure (even larger particle size) result in the higher ECSA by comparing C1 and C2 catalysts.

For C1 catalysts, such as CP3 and CP5 samples annealing at lower temperature, the first cyclic voltammograms show no hydrogen adsorption/desorption (H_{ad}) between 0.05 and 0.4 V, but do show high Cu redox peaks in Figure 2, implying a Cu-rich surface. After the initial several cycles, the surface was roughly dealloyed, and the Cu redox peaks decreased in intensity. From the 4th to 250th cycles, the H_{upd} region for CP3 has a minor increase (about 4%) and then decreases (Figure 3a). At the beginning, the increase in the ECSA for CP3 and CP5 should be attributed to depletion of the surface Cu and more exposed Pt surface sites. The Pt rough surface form and the coordination number of surface Pt is lowered because of the leaching of surface Cu atoms.[2,18] Under these conditions, the surface Pt atoms with low coordination numbers rearrange to reduce the number of dangling bonds (Figure 3e).[23] Moreover, the low coordination atoms are preferential sites for the adsorption of oxygenated species, and these sites are more vulnerable for dissolution, migration, and rearrangement.[41] Thus, after depletion of surface Cu atoms, the following potential cycling will induce the decrease in the ECSA (Figure 4a, b, e). This case is very similar to that of tiny particles with low coordination number growing into large particles to decrease the surface energy under potential cycling.[16]

For C2 catalysts, such as CP6 and CP7 samples annealing at higher temperature, the particles ripen and grow into a large size, high lattice ordering, and Pt-rich surface (Figures 1a, 2a and b, and Supporting Information Figures S2d and S5). The first cyclic voltammograms show no hydrogen adsorption/desorption (H_{ad}) between 0.05 and 0.4 V and low Cu redox

dx.doi.org/10.1021/cs300058c | ACS Catal. 2012, 2, 916−924

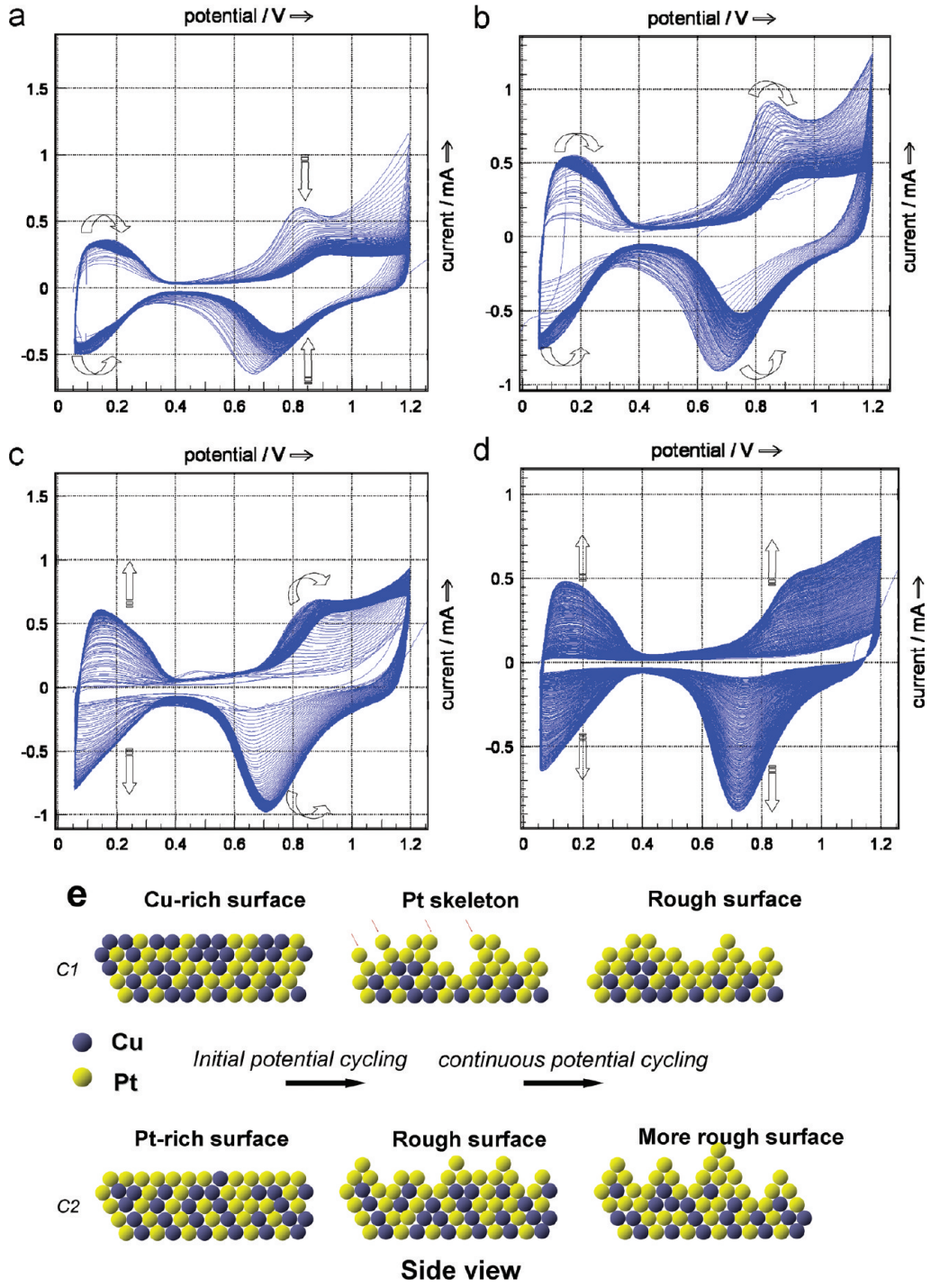

Figure 3. CVs original data of CuPt catalysts: (a) CP3, (b) CP5, (c) CP6, and (d) CP7. The experiments were performed in Ar-saturated 0.1 M $HClO_4$ solutions with a fast sweep rate of 250 mV/s and the data were recorded from the fourth to 250th cycles. (e) Schematic of different surface morphology evolutions between C1 and C2 catalysts. The red arrows show the dangling bonds.

peaks in Figure 2, implying few Pt active sites. Large particles normally have a small initial ECSA. After several initial cycles, the ECSA is still quite low (Figure 3c and d). It suggests that the ECSAs of CP6 and CP7 with a Pt-rich surface could not increase as the Cu-rich surface because fewer Cu atoms were leached out from the surface. However, the cycling was continually performed; the H_{ad} increased slowly but continuously (Figure 3c and d); and finally, the ECSA exceeded those of the CP3 and CP5 after 250 cycles, suggesting the large enhancement of the ECSA (Figure 5a and c).

As discussed above, after leaching of surface Cu, the Cu atoms from the subsurface and core region migrate to the top surface and dissolve. However, the surface segregation process is a relatively slow process,[15] and the fewest Cu atoms are dissolved from the particles after cycling in Figure 4. It implies that the enhanced ECSA may not only be attributed to the leaching of Cu. For these Pt shell particles, during the surface Cu leaching, the adsorbate-induced rearrangement of the surface Pt atoms may be present as discussed by Somorjai et al. in 1989.[23]

dx.doi.org/10.1021/cs300058c | ACS Catal. 2012, 2, 916−924

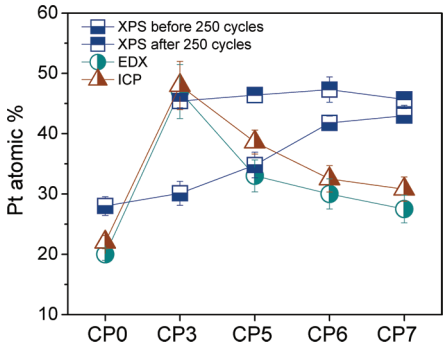

Figure 4. The Pt atomic fraction before and after cycling. The Pt atomic fraction in the surface region before and after cycling was measured by XPS. The chemical compositions in all were measured by energy-dispersive X-ray spectroscopy and inductively coupled plasma mass spectrometry.

As shown in Figure 1b, the TEM image demonstrates the obvious gullylike contrast difference, in contrast to the surface before cycling in Figure 1a, indicating the formation of a highly rough surface (Figure 1c). In addition, the TEM images also show that the particles have been welded together and the crystal boundaries disappear after cycling. These results indicate the intensive migration of Pt atoms upon cycling. The electron diffraction (ED) insets in Figure 1 show the disappearance of larger spacing facets of Cu_3Pt (100) and Cu_3Pt (110), revealing the absence of the ordered lattice, which may be caused by leaching of Cu at the Cu-rich (100) and (110) surfaces of $L1_2$ Cu_3Pt[42,43] and the relatively stronger surface segregation of these facets.[44] The potential cycling may cause a domino effect on order−disorder structural change and the disruption of near-surface ordering resulting from the absence of neighboring atoms.[39,45] The ED pattern after cycling becomes continuous, suggesting a morphology change. Compared with the ECSA of CP3, the ECSA was improved nearly 2 times (Figure 5c). Moreover, the CVs in Figure 3d indicate that the ECSA of CP7 has been largely improved compared with the initial cleaned surface area of the same sample. The ECSA for CP6 with an average particle size of 40 nm is 32.3 $m^2\ g_{Pt}^{-1}$; for CP7 with a particle size ~80 nm, it is 31.8 $m^2\ g_{Pt}^{-1}$ Pt. These results indicate that the increase of the ECSA results from the surface leaching of Cu and morphology restructuring-induced surface roughness.

3.4. ORR Activity. The electrocatalytic activities of CuPt porous tubular catalysts toward the ORR were studied. The ORR activities were conducted in O_2-saturated 0.1 M $HClO_4$ aqueous solutions on a glass carbon rotating disk electrode. Polarization curves for the ORR of these catalysts are shown in Figure 5b. The specific activity for CP6 is 0.8 mA cm^{-2} at 0.9 V, and it was shown to be 5-fold more active for ORR than that of the CP3 catalyst (Figure 5d). Here, polycrystalline Pt is selected as a common reference point for comparison. The specific activity of polycrystalline Pt is ~1.1 ± 0.1 mA cm^{-2} (Supporting Information Figure S6), which is consistent with the value reported by Mayrhofer et al.[46] The CP6 catalyst demonstrated a mass activity of 0.232 A mg_{Pt}^{-1} at 0.9 V, which was a 7-fold higher activity than that of the CP3 catalyst (0.03 A mg_{Pt}^{-1}). These results indicate that the rearranged Pt surfaces show a relatively high activity.

According to the relationship between lattice strain and the adsorbate bond energy reported by Strasser and co-workers,[5] a larger atomic fraction of Cu at the core will induce a higher lattice strain and, thus, reduce the binding energy of intermediate oxygenated adsorbates. In this study, compared with the C2 catalysts (CP6 and CP7) after 250 hostile potential

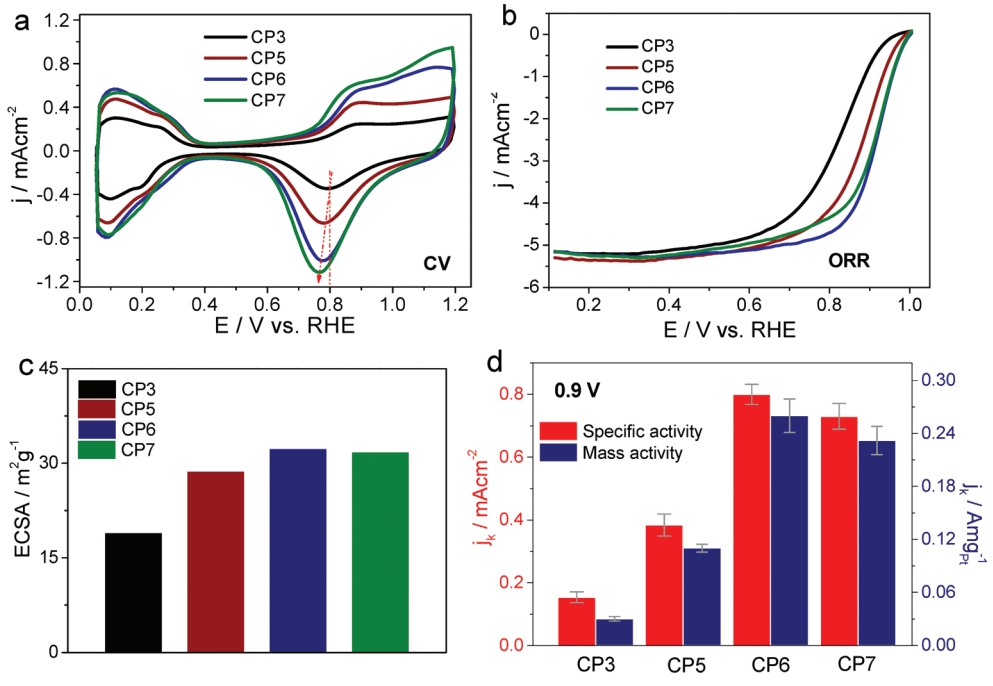

Figure 5. (a) CVs of the CuPt catalysts recorded in an Ar-saturated 0.1 M $HClO_4$ solution with a sweep rate of 50 mV/s. The red arrow shows regular negative shifts of the peak potentials on the backward sweep. (b) ORR polarization curves for CuPt catalysts after 250 cycles in an O_2-saturated 0.1 M $HClO_4$ solution (20 mV/s, 1600 rpm). (c) ECSAs for CuPt catalysts after 250 cycles. (d) Specific and mass activities of CuPt catalysts at 0.9 V vs RHE. Specific and mass activities are depicted as kinetic current densities (j_k) normalized to the ECSA and loading Pt mass, respectively.

dx.doi.org/10.1021/cs300058c | ACS Catal. 2012, 2, 916−924

cycles, the C1 catalysts (CP3 and CP5) have a lower Cu content at the core, which limits the ORR activity. Therefore, the ORR activity increases with an increase in the Cu composition at the core in Figure 5d. However, after potential cycling, the CP7 sample has a larger Cu composition in the core region but shows a stronger binding energy because the peak potential for the CP7 has a negative shift in comparison with CP3 on the backward sweep in Figure 5a. This issue can be explained in that the surface is highly rough, is rich in corner and edge sites, and has many defect sites, which favor the adsorption of hydroxyl species.

Recently, Wong and co-workers reported that the specific activity was highly improved by removing the surface defect sites via an acid wash protocol.[9−11,13] The high density of surface defect sites for CP7 induced by morphology restructuring discourages further improvement of the performance. The slight decrease in the activity in Figure 5d for CP7 could be the overly high adsorption for hydroxyl species due to the high density of surface defect sits. Thus, the enhanced performance for CP6 results from a balance between the higher Cu content at the core and the high density of the surface defect sites. Therefore, in addition to the composition, the surface microstructure should be considered for the adsorbate bond energy.

3.5. Adsorbate-Induced Restructuring. To clarify whether hydroxyl species induce morphology restructuring, a confined potential cycling was studied. Above 0.5 V, the Cl_{ad} is displaced by OH_{ad}, and above 0.85 V, Pt−O may form in the electrolyte.[47] To confirm whether the OH_{ad} played a key role in restructuring, the potential confined cycling within the hydroxyl adsorption potential region between 0.5 and 0.85 V was performed at 100 mV/s with different cycles. After different cycles, the potential was changed to 0.05−1.2 V to record the CVs in Figure 6. The ECSA increases with increasing the cycle,

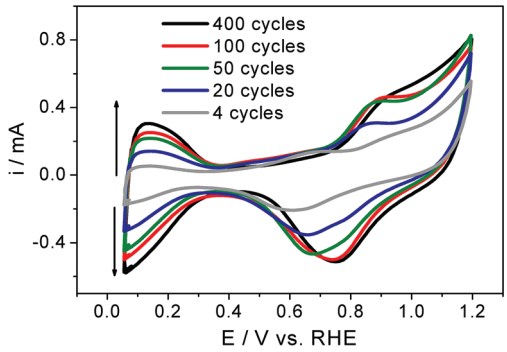

Figure 6. OH_{ad}-induced morphology restructuring. The potential-confined cycling was performed within the OH_{ad} region between 0.5 and 0.85 V vs RHE in Ar-saturated 0.1 M $HClO_4$ solution at 100 mV/s with different cycles. After different cycles, the potential was changed to between 0.05 and 1.2 V to record the CVs (250 mV/s).

which is the direct evidence that OH_{ad} can be one of the factors to induce restructuring and surface roughness. It must be pointed out that the covering of oxygenated species above 0.85 V may also contribute to the restructuring, but here we did not consider further. These results indicate that the OH_{ad} rebuild a highly active surface,[48] assisted by potential cycling, and the OH_{ad} may be acted as a "surgeon" to improve the active sites for catalytic reaction.

3.6. Stability and ECSA Restorability Test. The accelerated durability tests have been performed by linear potential sweeps between 0.6 and 1.0 V at 100 mV/s in O_2-saturated 0.1 M $HClO_4$ solutions at room temperature. After 4000 cycles, the results demonstrated a loss of 12.2% for the initial ECSA for the CP3 and 4.4% for the CP6 and surprisingly showed a gain of 4.5% for CP7 in Figure 7. After 10 000 cycles,

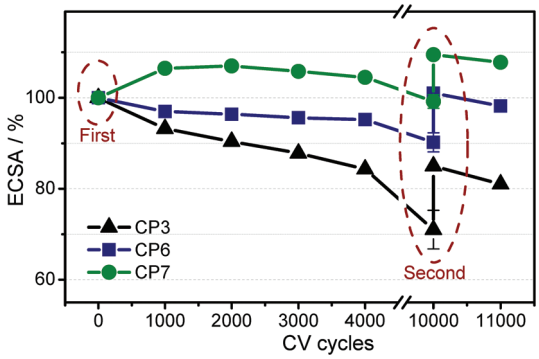

Figure 7. Stability and restorability test. The relative ECSA after the first 250 cycles was taken as 100% for comparison. The loss percentage of ECSA was obtained after a specified accelerated stability test. The stability test was performed in an O_2-saturated 0.1 M $HClO_4$ solution between 0.6 and 1.0 V (vs RHE) at 100 mV/s. After 10 000 cycles of the stability test, the second 250 cycles were performed to measure the restorability (the marked dashed lines represent how the catalysts performed for 250 cycles in Ar-saturated 0.1 M $HClO_4$ solution between 0.05 and 1.2 V with a sweep rate of 250 mV/s).

the CP7 catalyst showed almost no loss of the initial ECSA, and the stability of these CuPt catalysts displayed regular enhancement. Fuel cell catalysts in hostile electrolyte must suffer the harsh degradation due to the agglomeration, growth, loss and migration, and active site contamination of the Pt.[49] Therefore, the ECSAs of the particle catalysts are difficult to restore to the original level because of the degradation after removal of the surface contaminants. Here, after we replaced O_2-saturated with Ar-saturated 0.1 M $HClO_4$ solutions and performed another 250 cycles, the ECSA for CP6 and CP7 catalysts can be restored to the original level (Figure 7), but the CP3 cannot be restored completely. Thus, the highly improved stability and restorability could be due to the adsorbate-induced restructuring during potential cycling.[27]

As discussed above, the CuPt catalysts with a Cu-rich surface cause the leaching of Cu, and the coordination number of Pt on the surface decreases, and thus, the Pt atoms will rearrange to decrease the surface dangling bonds (ECSA decrease) in typical fuel cell application ranges, as demonstrated in Figure 3e. For CP7, the initial surface is a Pt shell with a high coordination number. The surface energy of the compressive strain Pt−Pt atoms on the surface may be high that induce rearrangement (ECSA increase) to decrease the surface strain by adsorbates in the electrolyte in Figure 3e. Thus, the rearranged surface should be more stable according to the energy principle.

4. CONCLUSIONS

This study demonstrated the design and synthesis of highly active and durable CuPt catalysts formed through potential cycling in acid electrolyte. When increasing the surface Pt atomic fraction and lattice ordering, fewer Cu atoms were leached out and dissolved into solution but a higher ECSA was obtained after potential cycling, which was explained by adsorbate-induced morphology restructuring and different surface configuration evolution. The adsorbate-induced mor-

dx.doi.org/10.1021/cs300058c | ACS Catal. 2012, 2, 916−924

phology restructuring can rebuild a highly rough surface, demonstrated by enhanced specific and mass activities of 0.8 mA cm_{Pt}^{-2} and 0.232 A mg_{Pt}^{-1} at 0.9 V for ORR and enhanced long-term stability. After 10 000 cycles, the C2 catalysts display almost no loss of the initial ECSA. Meanwhile, the stability of these CuPt catalysts shows regular change from C1 to C2 catalysts with increased Pt surface content and lattice ordering. Moreover, after a long-term stability measurement, the ECSA of the rearranged surface can be restored to its initial value after 250 cycles, and thus, this kind of electrocatalyst may be developed as a next-generation restorable cathode fuel cell catalyst. Therefore, this strategy provides new insight and understanding of catalytic activity enhancement and long-term stability for a platinum-based alloy system.

■ ASSOCIATED CONTENT

Supporting Information

HRTEM images and XPS data. This material is available free of charge via the Internet at http://pubs.acs.org.

■ AUTHOR INFORMATION

Corresponding Author

*Fax: (+) 86 551 3603040. E-mail: shyu@ustc.edu.cn.

Notes

The authors declare no competing financial interest.

■ ACKNOWLEDGMENTS

S. H. Yu acknowledges special funding support from the National Basic Research Program of China (No. 2010CB934700), the National Natural Science Foundation of China (Nos. 91022032, 21061160492, J1030412), Chinese Academy of Sciences (Grant KJZD-EW-M01-1), International Science & Technology Cooperation Program of China (No. 2010DFA41170), and the Principal Investigator Award by the National Synchrotron Radiation Laboratory at the University of Science and Technology of China.

■ REFERENCES

(1) Ji, X.; Lee, K. T.; Holden, R.; Zhang, L.; Zhang, J.; Botton, G. A.; Couillard, M.; Nazar, L. F. *Nat. Chem.* **2010**, *2*, 286−293.

(2) Stamenkovic, V. R.; Mun, B. S.; Arenz, M.; Mayrhofer, K. J. J.; Lucas, C. A.; Wang, G. F.; Ross, P. N.; Markovic, N. M. *Nat. Mater.* **2007**, *6*, 241−247.

(3) Xu, Y.; Ruban, A. V.; Mavrikakis, M. *J. Am. Chem. Soc.* **2004**, *126*, 4717−4725.

(4) Shuo, C.; Wenchao, S.; Yabuuchi, N.; Ferreira, P. J.; Allard, L. F.; Yang, S.-H. *J. Phys. Chem. C* **2009**, *113*, 1109−25.

(5) Strasser, P.; Koh, S.; Anniyev, T.; Greeley, J.; More, K.; Yu, C.; Liu, Z.; Kaya, S.; Nordlund, D.; Ogasawara, H.; Toney, M. F.; Nilsson, A. *Nat. Chem.* **2010**, *2*, 454−460.

(6) Adzic, R. R.; Zhang, J.; Sasaki, K.; Vukmirovic, M. B.; Shao, M.; Wang, J. X.; Nilekar, A. U.; Mavrikakis, M.; Valerio, J. A.; Uribe, F. *Top. Catal.* **2007**, *46*, 249−262.

(7) Zhou, W. P.; Yang, X. F.; Vukmirovic, M. B.; Koel, B. E.; Jiao, J.; Peng, G. W.; Mavrikakis, M.; Adzic, R. R. *J. Am. Chem. Soc.* **2009**, *131*, 12755−12762.

(8) Mayrhofer, K. J. J.; Juhart, V.; Hartl, K.; Hanzlik, M.; Arenz, M. *Angew. Chem., Int. Ed.* **2009**, *48*, 3529−3531.

(9) Koenigsmann, C.; Zhou, W. P.; Adzic, R. R.; Sutter, E.; Wong, S. S. *Nano Lett.* **2010**, *10*, 2806−2811.

(10) Koenigsmann, C.; Santulli, A. C.; Sutter, E.; Wong, S. S. *ACS Nano* **2011**, *5*, 7471−7487.

(11) Koenigsmann, C.; Santulli, A. C.; Gong, K.; Vukmirovic, M. B.; Zhou, W.-p.; Sutter, E.; Wong, S. S.; Adzic, R. R. *J. Am. Chem. Soc.* **2011**, *133*, 9783−9795.

(12) Zhou, H. J.; Zhou, W. P.; Adzic, R. R.; Wong, S. S. *J. Phys. Chem. C* **2009**, *113*, 5460−5466.

(13) Koenigsmann, C.; Wong, S. S. *Energy Environ. Sci.* **2011**, *4*, 1161−1176.

(14) Mayrhofer, K. J. J.; Ashton, S. J.; Meier, J. C.; Wiberg, G. K. H.; Hanzlik, M.; Arenz, M. *J. Power Sources* **2008**, *185*, 734−739.

(15) Mayrhofer, K. J. J.; Hartl, K.; Juhart, V.; Arenz, M. *J. Am. Chem. Soc.* **2009**, *131*, 16348−16349.

(16) Mayrhofer, K. J. J.; Blizanac, B. B.; Arenz, M.; Stamenkovic, V. R.; Ross, P. N.; Markovic, N. M. *J. Phys. Chem. B* **2005**, *109*, 14433−14440.

(17) Wang, C.; Chi, M.; Wang, G.; van der Vliet, D.; Li, D.; More, K.; Wang, H.-H.; Schlueter, J. A.; Markovic, N. M.; Stamenkovic, V. R. *Adv. Funct. Mater.* **2011**, *21*, 147−152.

(18) Stamenkovic, V. R.; Mun, B. S.; Mayrhofer, K. J. J.; Ross, P. N.; Markovic, N. M. *J. Am. Chem. Soc.* **2006**, *128*, 8813−8819.

(19) Tao, F.; Salmeron, M. *Science* **2011**, *331*, 171−174.

(20) Tao, F.; Grass, M. E.; Zhang, Y. W.; Butcher, D. R.; Renzas, J. R.; Liu, Z.; Chung, J. Y.; Mun, B. S.; Salmeron, M.; Somorjai, G. A. *Science* **2008**, *322*, 932−934.

(21) Wang, J. X.; Inada, H.; Wu, L. J.; Zhu, Y. M.; Choi, Y. M.; Liu, P.; Zhou, W. P.; Adzic, R. R. *J. Am. Chem. Soc.* **2009**, *131*, 17298−17302.

(22) Tao, F.; Grass, M. E.; Zhang, Y. W.; Butcher, D. R.; Aksoy, F.; Aloni, S.; Altoe, V.; Alayoglu, S.; Renzas, J. R.; Tsung, C. K.; Zhu, Z. W.; Liu, Z.; Salmeron, M.; Somorjai, G. A. *J. Am. Chem. Soc.* **2010**, *132*, 8697−8703.

(23) Somorjai, G. A.; Van Hove, M. A. *Prog. Surf. Sci.* **1989**, *30*, 201−231.

(24) Tao, F.; Dag, S.; Wang, L. W.; Liu, Z.; Butcher, D. R.; Bluhm, H.; Salmeron, M.; Somorjai, G. A. *Science* **2010**, *327*, 850−853.

(25) Tao, F.; Dag, S.; Wang, L. W.; Liu, Z.; Butcher, D. R.; Salmeron, M.; Somorjai, G. A. *Nano Lett.* **2009**, *9*, 2167−2171.

(26) Ibach, H. *Surf. Sci. Rep.* **1997**, *29*, 195−263.

(27) Cui, C. H.; Li, H. H.; Yu, S. H. *Chem. Sci.* **2011**, *2*, 1611−1614.

(28) Mohl, M.; Dobo, D.; Kukovecz, A.; Konya, Z.; Kordas, K.; Wei, J.; Vajtai, R.; Ajayan, P. M. *J. Phys. Chem. C* **2011**, *115*, 9403−9409.

(29) Larsen, B. A.; Pylypenko, S.; Olson, T.; Neyerlin, K. C.; Pivovar, B. *ECS Meeting Abstracts* **2010**, *1002*, 1972−1972.

(30) Tan, Y.; Fan, J.; Chen, G.; Zheng, N.; Xie, Q. *Chem. Commun.* **2011**, *47*, 11624−1162.

(31) Liu, L.; Pippel, E. *Angew. Chem., Int. Ed.* **2011**, *50*, 2729−2733.

(32) Chen, Z. W.; Waje, M.; Li, W. Z.; Yan, Y. S. *Angew. Chem., Int. Ed.* **2007**, *46*, 4060−4063.

(33) Cui, C. H.; Li, H. H.; Yu, J. W.; Gao, M. R.; Yu, S. H. *Angew. Chem., Int. Ed.* **2010**, *49*, 9149−9152.

(34) Cui, C. H.; Li, H. H.; Yu, S. H. *Chem. Commun.* **2010**, *46*, 940−942.

(35) Zhou, S. H.; Varughese, B.; Eichhorn, B.; Jackson, G.; McIlwrath, K. *Angew. Chem., Int. Ed.* **2005**, *44*, 4539−4543.

(36) *Binary Alloy Phase Diagrams*, 2nd ed.; Massalski, T. B., Okamoto, H., Subramanian, P. R., Kacprzak, L., Eds.; ASM International: Materials Park, OH, 1990; Vol. 2; pp 1460−1462.

(37) Strasser, P.; Koha, S.; Greeley, J. *Phys. Chem. Chem. Phys.* **2008**, *10*, 3670−3683.

(38) Huang, W. J.; Sun, R.; Tao, J.; Menard, L. D.; Nuzzo, R. G.; Zuo, J. M. *Nat. Mater.* **2008**, *7*, 308−313.

(39) Polak, M.; Rubinovich, L. *Surf. Sci. Rep.* **2000**, *38*, 127−194.

(40) Lim, B.; Jiang, M.; Camargo, P. H. C.; Cho, E. C.; Tao, J.; Lu, X.; Zhu, Y.; Xia, Y. *Science* **2009**, *324*, 1302−1305.

(41) Wang, C.; Chi, M.; Li, D.; Strmcnik, D.; van der Vliet, D.; Wang, G.; Komanicky, V.; Chang, K.-C.; Paulikas, A. P.; Tripkovic, D.; Pearson, J.; More, K. L.; Markovic, N. M.; Stamenkovic, V. R. *J. Am. Chem. Soc.* **2011**, *133*, 14396−14403.

(42) Schurmans, M.; Luyten, J.; Creemers, C.; Declerck, R.; Waroquier, M. *Phys. Rev. B* **2007**, *76*, 174208.

(43) Shen, Y. G.; O'Connor, D. J.; Wandelt, K. *Surf. Sci.* **1998**, *410*, 1−14.

(44) Müller, M.; Albe, K. *Phys. Rev. B* **2005**, *72*, 094203.

(45) Saha, D. K.; Ohshima, K. *J. Phys.: Condens. Matter* **1993**, *5*, 4099−4110.
(46) Mayrhofer, K. J. J.; Strmcnik, D.; Blizanac, B. B.; Stamenkovic, V.; Arenz, M.; Markovic, N. M. *Electrochim. Acta* **2008**, *53*, 3181−3188.
(47) Markovic, N. M.; Ross, P. N. *Surf. Sci. Rep.* **2002**, *45*, 121−229.
(48) Lucas, C. A.; Markovicacute, N. M.; Ross, P. N. *Phys. Rev. Lett.* **1996**, *77*, 4922.
(49) Liang, H.-W.; Cao, X.; Zhou, F.; Cui, C.-H.; Zhang, W.-J.; Yu, S.-H. *Adv. Mater.* **2011**, *23*, 1467−1471.